JSR Publications

Available Online

J. Sci. Res. **18** (1), 231-240 (2026)

JOURNAL OF SCIENTIFIC RESEARCH

www.banglajol.info/index.php/JSR

3-Chloro-5-(trifluoromethyl)benzonitrile: Spectroscopic Progression and Evaluation by Density Functional Theory

S. Valli Chitra[1*], A. Sankar[2], K. Parimala[3]

[1]Department of Chemistry, Government Arts College for Women, Krishnagiri-635002, Tamilnadu, India

[2]Department of Chemistry, Kandaswami Kandar's College, P. Velur-638182, Tamilnadu, India

[3]PG & Research Department of Physics, Nehru Memorial College, Trichy-621007, Tamilnadu, India

Received 10 August 2025, accepted in final revised form 8 October 2025

Abstract

The FT-IR and FT-Raman spectra of 3-chloro-5-(trifluoromethyl)benzonitrile (TFMBN) are analysed using the hybrid correlation approach. Using density functional theory, B3LYP and the 6-311++G(d,p) basis set were utilised to determine the molecular structure, vibrational wavenumbers, infrared intensities, and Raman activities. The computational model's dependability was validated by comparing experimental and theoretical vibrational frequencies. The stability and chemical reactivity of the molecule were confirmed by the FMO orbital analysis, which also measured the energy gap between the HOMO and LUMO. The computed frequencies were also used to determine thermodynamic parameters, including heat capacity, entropies, enthalpy, and their relationships with temperatures.

Keywords: TFMBN; FT-IR; FT-Raman; B3LYP.

doi: https://dx.doi.org/10.3329/jsr.v18i1.83645 J. Sci. Res. **18** (1), 231-240 (2026)

1. Introduction

Benzonitrile has a flash point of 71.6 °C and is a clear, colorless liquid with an almond-like smell. Water, a unique solvent used to create other chemicals, dissolves benzonitrile less readily. Many anhydrous metallic salts, polymers, specialized lacquers, nitrile rubber, and resins can be effectively dissolved in benzotrimethyl ether. Furthermore, through the processes of nitration, halogenation, condensation, esterification, hydrolysis, and alkylation, it is regarded as a major solvent that serves as a chemical transition for the synthesis of rubber compounds, dyestuffs, and medicines [1]. Additionally, it serves as a flexible precursor to several derivatives. In addition to serving as intermediates for agrochemicals, medications, and other organic compounds, benzonitrile derivatives are utilized to create polymers, lacquers, and anhydrous metallic salts. Several research

* *Corresponding author:* valliap29@gmail.com

investigations have examined the harmful consequences of 4-hydroxybenzonitrile, a compound that has antifungal [2] and insecticidal properties [3,4].

The pharmaceutical and synthetic organic industries use 4-acetylbenzonitrile. 4-Formyl benzonitrile serves as a bridge in the fields of pharmacy, liquid crystals, and organic synthesis. Transition metals and benzonitrile can combine to form coordination complexes that are conveniently soluble in organic solvents. Because stronger ligands can readily replace benzonitrile ligands, benzonitrile complexes are helpful synthetic intermediates. Because of its unique physical and biological characteristics, research has been done on the benzonitrile molecule and a few of its variants [5-7]. Regarding the vibrations and structural characteristics of benzonitrile and its radical anion vibrational spectra, Dimitrova [8] studied 4-formylbenzonitrile and 4-bromobenzonitrile. The compounds 4-acetylbenzonitrile, 4-formylbenzonitrile, and 4-hydroxybenzonitrile are significant from a theoretical perspective [9,10]. The purpose of this work is to characterize the 3-Chloro-5-(trifluoromethyl)benzonitrile (TFMBN) and then use DFT calculations to study its molecular properties. By utilizing the HOMO-LUMO analysis, one can determine the bioactive property of the molecule by calculating its band gap energy.

2. Materials and Methods

2.1. Methodology

The best chemical, 3-Chloro-5-(trifluoromethyl)benzonitrile (TFMBN), was used for each application. The FT-IR spectrum is obtained by using a PERKIN ELMER FT-IR spectrometer that operates at 1.0 cm^{-1} resolution and covers the 4000–400 cm^{-1} range. The KBr pellet technique's discharge mode is used to obtain the FT-IR spectrum. A Bruker RFS 27 spectrometer operating in the 4000–100 cm^{-1} range was used to produce the FT-Raman spectrum of the Neodymium-doped Yttrium Aluminium Garnet (Nd-YAG) laser, which was operated at 200 mW power.

2.2. *Computational details*

The Gaussian 9W package uses the molecular structure computation [11,12]. The molecular properties were computed using Becke's three-parameter hybrid functional (B3) [13,14] together with the gradient-corrected correlation functional of Lee-Yang-Parr (LYP) [15] with the 6-311++G(d,p) basic set. Vibrational wavenumbers and thermodynamic analysis were calculated using the optimized structural parameters. The normal modes of assignment have been verified and visually animated using Sundius's proposed MOLVIB program (Version 7.0-G77) [16].

3. Results and Discussion

3.1. *Molecular structure and vibrational analysis*

The optimized molecular structure and atom numbering of the present molecule were presented in Fig. 1. The TFMBN molecular structure is a member of the C1 point group symmetry. With 16 atoms, the title compound possesses 42 significant vibrations, including 13 out-of-plane and 29 in-plane vibrations. A molecule consists of 8 C atoms, 1 N atom, 1 Cl atom, 3 H atoms and 3 F atoms constituted in a selected compound. Both the FT-IR and FT-Raman spectra revealed every vibration that was anticipated for the molecule.

Fig. 1. Molecular structure of TFMBN with atom.

The Gaussian 9W package with the B3LYP/6-311++G(d,p) method was used for understanding the vibrational wavenumbers and their vibrations. This vibration was also determined at FT-IR and FT-Raman, with the experimental and theoretical values along with the contribution of TED values observed by the B3LYP/6-311++G(d,p) level. The wavenumber allocations of the studied molecule were noted in Table 1. Figs. 2 and 3 display the theoretical and experimental findings of the FT-IR and FT-Raman spectra. The total energy distribution and spectral wavenumbers for each normal mode have been established using the B3LYP technique with a scaling factor of 0.961.

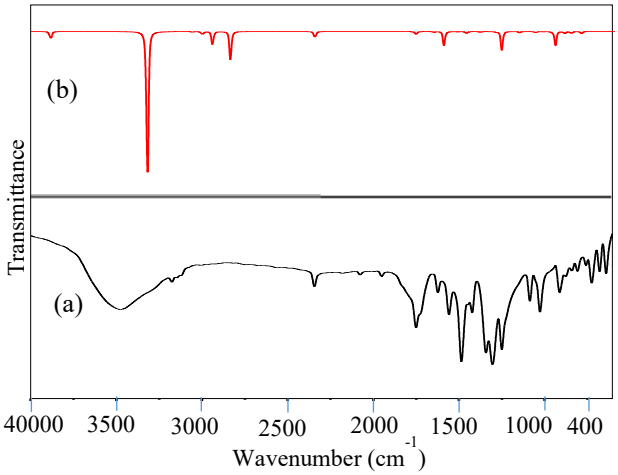

Fig. 2. FT-IR spectrum of TFMBN (a) observed and (b) calculated.

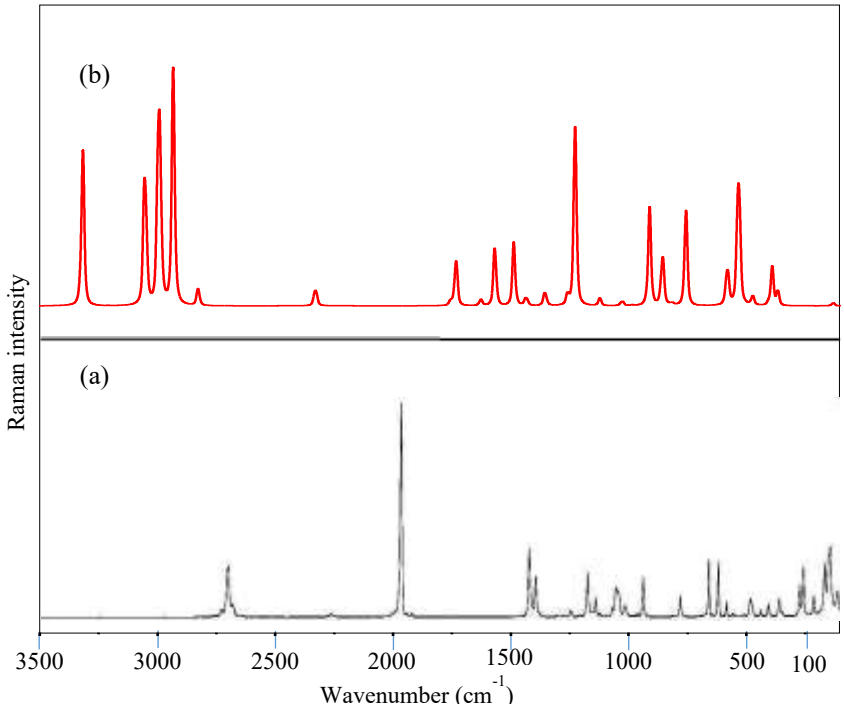

Fig. 3. FT-Raman spectrum of TFMBN (a) observed and (b) calculated.

3.2. *C–H vibrations*

The skeletal stretching of the benzene ring's C–H vibrations is typically found around the 3100–3000 cm^{-1} region [17,18]. While mode 3 is inactive in FT-Raman, the other two of the three anticipated C–H stretching vibration modes 1, 2, and 3 are seen as faint and extremely weak peaks in the FT-IR spectrum at 3500 and 3250 cm^{-1}. Tri-substituted benzene derivatives' C–H in-plane bending modes define normal vibrations 16, 17, and 19. The third mode, which is inactive in both Raman and infrared, is seen in the area around 1300 cm^{-1} [17].

Although the scaled value is at 1185 cm^{-1}, the C–H in-plane bending mode 3 is active in both Raman and infrared. Three modes are seen as very weak and medium bands at 1250, 1200, and 1040 cm^{-1} in the FT-Raman spectrum, whereas modes 16 and 19 are shown as strong bands in the FT-IR spectrum. Experimental results and the theoretically determined C–H in-plane bending vibrations of 1193, 1127, and 945 cm^{-1} show excellent agreement. The TFMBN's C–H in-plane and out-of-plane bending vibrations are responsible for the spectral reach.

Table 1. Vibrational assignments of fundamental frequencies are obtained for TFMBN using B3LYP/6-311++G(d,p) level of theory.

Sl.No.	Observed frequencies (cm^{-1})		Calculated frequencies (cm^{-1})		[a]IR	[b]Raman	Vibrational assignments with >10 % of TED
	FT-IR	FT-Raman	Unscaled	Scaled			
1	3500(w)		3558	3478	120	56	νC–H (100)
2	3250(vw)		3297	3129	262	23	νC–H (99)
3			3036	2945	10	24	νC–H (98)
4			2983	2815	14	64	CF3 asym (89)
5			2974	2729	32	100	CF3 asym (84)
6			2918	2658	192	74	CF3 sym (83)
7		1980(vs)	1914	1813	426	12	νC–C (85)
8			1824	1754	106	13	νC–C (83)
9	1750(vs)		1760	1673	3	2	νC–C (81)
10	1700(m)		1737	1594	41	26	νC–C (81)
11			1634	1517	11	3	νC–C (80)
12	1580(s)		1574	1423	200	29	νC–C (75)
13	1500(vs)		1495	1384	4	30	νC–C (74)
14		1420(s)	1444	1329	33	5	νC–C (72)
15	1380(vw)	1400(m)	1365	1256	11	8	νC–N (76)
16	1250(s)	1250(vw)	1270	1193	8	5	bC–H (71)
17		1200(m)	1239	1127	260	81	bC–H (73)
18	1100(m)	1180(w)	1136	1093	17	3	CF3 ipb (68)
19	1020(s)	1040(vw)	1043	945	21	3	bC–H (63)
20			1001	823	2	4	νC–Cl (64)
21		940(m)	946	792	9	3	CF3 opb (53)
22			928	735	188	41	CF3 sb (54)
23			874	695	30	26	CF3 ipr (52)
24	800(m)		835	641	31	1	CF3 opr (50)
25		780(w)	776	611	25	38	ωC–H (59)
26	600(vw)	620(s)	603	572	9	19	ωC–H (53)
27		590(vw)	556	523	5	70	bC–N (78)
28		490(w)	497	485	15	4	ωC–H (59)
29			432	445	8	7	bC–C (78)
30	400(m)		416	402	12	14	bC–C (67)
31		390(vw)	392	345	8	5	bC–Cl (78)
32			361	302	1	1	bC–C (78)
33			345	284	2	3	bC–C (67)
34			315	242	24	16	bC–C (78)
35			300	205	8	3	ωC–C (57)
36			283	191	16	19	ωC–C (55)
37			265	162	2	3	ωC–Cl (57)
38		240(w)	243	123	1	11	ωC–N (57)
39		215(w)	212	105	23	1	ωC–C (55)
40			198	85	4	5	ωC–C (57)
41			155	64	1	4	ωC–C (55)
42		120(s)	125	45	15	4	tCF3 (44)

Experimental relative intensities are abbreviated as follows: vs-very strong, s-strong, m-medium, w-weak, vw-very weak, [a]IR- intensities, [b]Raman- Raman activities. Abbreviations; ν-stretching, sym-symmetric stretching, asym-asymmetric stretching, b-in-plane bending, ω-out-of-plane bending, ipb-in-plane bending, opb-out-of-plane bending, sb-symmetric bending, ipr-in-plane rock, opr-out-of-plane rock, t-torsion.

3.3. *Ring vibrations*

The aromatic C–C stretching vibration takes place between 1589 and 1301 cm^{-1} [18]. Theoretically, C–C stretching vibrations are responsible for the frequencies seen in the FT-IR spectrum at 1750 (vs), 1700 (m), 1580 (s), and 1500 (vs) cm^{-1}; the FT-Raman spectrum at 1980 (vs) and 1420 (s) cm^{-1}; and the 1813–1329 cm^{-1} value in the current study. According to predictions, the out-of-plane vibrations have been detected at lower frequencies than the in-plane deformations. Moreover, there is a good correspondence between the experimental observations and the two bending modes.

3.4. *CN group vibrations*

The C≡N stretching absorption is strong and detected in the restricted band between 2260 and 2200 cm^{-1} [17]. When it comes to benzonitrile compounds, conjugation takes place, which lowers the frequency of C≡N absorption to 2240–2200 cm^{-1}. The type of substituents has little effect on the bands in this area [19]. The C≡N stretching mode of TFMBN has a medium and extremely weak intensity. The FT-IR and FT-Raman spectra of TFMBN show the C≡N stretching band at 1380 cm^{-1} and 1400 cm^{-1}, respectively. Excellent agreement is found between experimental data and the theoretically determined C≡N stretching vibration of 1256 cm^{-1}. There are in-plane and out-of-plane bending peaks at 590 cm^{-1} and 240 cm^{-1} in the FT-Raman spectrum.

3.5. *CF_3 vibrations*

The CF_3 stretching vibrations are typically symmetric and asymmetric, with ranges of 1270–1235 cm^{-1} and 1226–1200 cm^{-1}, respectively [20,21]. Both the symmetric and asymmetric stretching vibrations of the CF_3 group are present in the active FT-IR and FT-Raman spectra, and the B3LYP technique theoretically calculates them to be 2815, 2729, and 2658 cm^{-1}. The most common locations for the CF deformation vibrations are 695–635 cm^{-1}, 644–583 cm^{-1}, and 592–495 cm^{-1} [21,22].

As a result, the FT-IR spectrum of TFMBN shows CF_3 ipb and CF_3 opb vibrations at 1100 cm^{-1}, while the spectrum of the FT-Raman spectrum shows them at 1180 and 940 cm^{-1}. The literature supports the aforementioned values [23,24]. The FT-IR spectrum's 800 cm^{-1} band is assigned to the CF_3 asymmetric rocking state. The torsional motion in the spectra is hard to see. This is partially due to the strong rotational band intensities and the low wavenumber of the CF_3 torsional absorption.

3.6. *C–Cl vibrations*

The aromatic C–Cl stretching frequency was seen within the 800–600 cm^{-1} range in derivatives of benzene that contain a Cl atom [17]. Theoretically, the C–Cl stretching mode is assigned to the frequency 823 cm^{-1}. In 2-A, 5-CB, it is challenging to assign the C–Cl

deformation mode with wavenumbers expected below 400 cm^{-1} [24] for two reasons: first, the region's Raman spectral lines are generally weak, and second, the infrared range does not extend below 200 cm^{-1}. In this case, the highly deficient FT-Raman band at 390 cm^{-1} shows the in-plane asymmetric state of C–Cl. In this case, the C–Cl out-of-plane bending modes are comfortably inside the expected limits [17].

3.7. *Global reactivity descriptors*

The following are components of chemical potential: electronegativity, chemical hardness, ionization potential, energy gap, electron affinity, chemical softness, lowest unoccupied molecular orbital energy, and highest occupied molecular orbital energy (EHOMO) [25]. The energy gap (Eg) was the defining characteristic of a molecule's chemical reactivity. Reduced energy gaps promote charge transfer within the ligand, as demonstrated by the results [26,27]. Table 2 displays the calculated parameters. The exceptionally low (η) value for the title molecule suggests that the investigation can transfer charge. A lower global nucleophilicity index and a greater global electrophilicity index are indicative of more reactive chemicals, respectively.

If the electron affinity value is low, then the molecular reactivity to nucleophiles is high. S = 4.1766 eV and η = 3.8513 eV are the computed values for softness and hardness, correspondingly. The chemical softness and hardness of a named molecule are related to its band gap energy. At ϋ = 0.2724 eV, the electrophilicity index is calculated to show the biological activity of the molecule. The fact that the chemical potential of the molecule is negative (ν = -3.9679 eV) indicates that it is stable. With their corresponding energy gaps at 4.4665 eV, the chemical activity can be seen in the LUMO and HOMO energy values.

Table 2. Calculation of various electronic properties of compound TFMBN such as E_{LUMO}, E_{HOMO}, (E_{LUMO} - E_{HOMO}), V, A, η, S, χ, μ, and ω in eV by using B3LYP/6-311++G(d,p) level.

Parameters	B3LYP
HOMO energy (EHOMO) (eV)	–5.4734
LUMO energy (ELUMO) (eV)	–1.0069
Band gap (Eg) (eV)	4.4665
Ionization potential (V) (eV)	5.8958
Electron affinity (A) (eV)	2.1342
Chemical hardness (η) (eV)	3.8513
Chemical softness (S) (eV^{-1})	4.1766
Electronegativity (χ) (eV)	3.9784
Chemical potential (μ) (eV)	–3.9679
Electrophilicity (ω) (eV)	0.2724

3.8. *Frontier molecular orbital analysis*

When interacting with other species, the molecule's boundary molecular orbitals are what really matter. Molecular orbitals, both occupied and unoccupied, are shown in three dimensions in Fig. 4. The groups of electrons classified as donors and acceptors are HOMO

and LUMO, respectively [28]. By applying Koopman's theorem, one may determine the border molecular orbital [29]. The energy difference of 4.4665 eV between the HOMO and the LUMO is one key element affecting electron conductivity, as seen in Fig. 4. A molecular charge transfer interaction can be understood by comparing the energy gaps of the HOMO-LUMO and HOMO-1-LUMO+1 states.

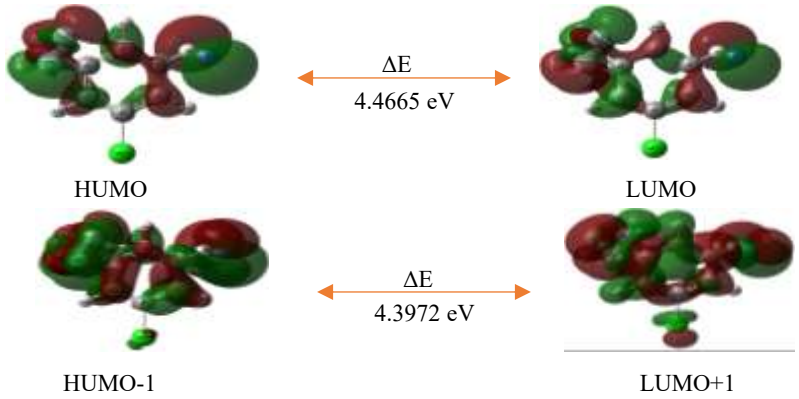

Fig. 4. FMOs like highest occupied molecular orbitals and lowest unoccupied molecular orbitals of TFMBN.

3.9. *Thermodynamic properties*

Based on vibrational research, we calculated the statically thermodynamic functions of the TFMBN molecule from its theoretical frequencies. The following are displayed in Table 3: entropy (S), heat capacity (Cp), changes in enthalpy (H-E/T), and Gibbs free energy (G-E/T). Table 3 shows that all thermodynamic functions, with the exception of Gibbs's free energy, grow with temperatures between 100 and 1000 K because, as one would expect, the vibrational intensities of all molecules do as well with temperatures. Results for the correlation coefficients of enthalpy changes, temperatures, heat capacity, Gibbs free energy, and entropy were best fit by quadratic formulae. Fitting factors (R^2) of 0.999 and 1.000, respectively, are related with these thermodynamic features. See the following in Fig. 13 for the correlation pictures of the relevant fitting equations (1–4).

$C_p = 3.234 + 0.301T – 0.008T^2$ ($R^2 = 0.999$) (1)

$(H-E)/T = 0.574 + 0.265T – 0.006T^2$ ($R^2 = 0.999$) (2)

$(G-E)/T = - 56.69 - 0.132T – 0.003T^2$ ($R^2 = 0.999$) (3)

$S = 57.19 + 0.281T – 0.004T^2$ ($R^2 = 1.000$) (4)

All the data interpreted in thermodynamics are effective, and that can be taken to further analysis on the TFMBN. The interpreted data is utilized in the thermodynamical field to approximate the molecular principal processes in conformity with the thermodynamics' second law. Find a few more thermodynamic energies associated with the association of the thermodynamic functions.

Table 3. Thermodynamic properties of TFMBN at different temperatures calculated by B3LYP/6-311++G(d,p) method.

Temp (K)	Cp (calmol^{-1} K^{-1})	(H-E)/T (kcal mol^{-1})	S (kcal mol^{-1})	(G-E)/T (kcal mol^{-1})
100	12.678	2.059	66.539	–74.527
200	21.975	6.827	72.797	–79.898
300	27.074	5.039	75.458	–83.648
400	38.269	7.976	83.854	–95.426
500	54.034	23.279	108.645	–103.871
600	58.376	28.157	116.569	–105.825
700	53.591	25.518	125.798	–117.341
800	72.495	31.571	135.992	–123.651
900	65.906	35.956	137.395	–129.452
1000	75.439	37.665	147.768	–135.205

4. Conclusion

The B3LYP/6-311++G(d,p) approach is used in this study's computation to optimise the TFMBN's molecular structure and harmonic wavenumbers. FT-IR and FT-Raman spectra of the title molecule were in agreement with the theoretical vibrational assignments obtained from regular coordinate discussion. The chemical reactive sites are also identified by the FMO analysis, and the HOMO and LUMO energies, along with their gap, are determined to be 4.4665 eV. The correlations between the statistical thermodynamics properties and temperature are also obtained. It is seen that the heat capacity, entropy, enthalpy, Gibb's free energy increases with the increasing of temperature owing to the intensities of the molecular vibrations increase with increasing temperature.

References

1. V. A. Shenai, Chemistry of Dyes and Principles of Dyeing (Sevak Publications, Mumbai, 1995).
2. A. G. Rütgerswerke and H. G. Franck, Industrial Aromatic Chemistry: Raw Materials Processes. Products, 1st Edition (Springer-Verlag Berlin, Heidelberg, 1988).
3. T. R. Fukuto and R. L. Metcalf, J. Agric. Food Chem. **4**, 930 (1956). https://doi.org/10.1021/jf60069a001
4. T. W. Schultz, Ecotoxicol. Environ. Saf. **14**, 178 (1987). https://doi.org/10.1016/0147-6513(87)90060-1
5. T. Konishi, M. Fujitsuka, O. Ito, Y. Toba, and Y. Usui, Bull. Chem. Soc. Japan **74**, 39 (2001). https://doi.org/10.1246/bcsj.74.39
6. A. S. R. Koti and N. Periasamy, Res. Chem. Intermed. **28**, 831 (2002). https://doi.org/10.1163/15685670260469447
7. Y. I. Binev, J. Mol. Struct. (Theochem.) **535**, 93 (2001). https://doi.org/10.1016/S0166-1280(00)00577-7
8. Y. Dimitrova, J. Mol. Struct. (Theochem.) **391**, 241 (1997). https://doi.org/10.1016/S0166-1280(96)04813-0
9. V. Arjunan, K. Carthigayan, S. Periandy, K. Balamurugan, and S. Mohan, Spectrochim. Acta **98 A**, 156 (2012). https://doi.org/10.1016/j.saa.2012.08.053

10. B. H. Loo, Y. G. Lee, and D. O. Frazier, Chem. Phys. Lett. **119**, 312 (1985). https://doi.org/10.1016/0009-2614(85)80423-1
11. M. J. Frisch, G. W. Trucks, H. B. Schlegel, G. E. Scuseria, M. A. Robb et al., Gaussian Inc. Gaussian 09 Revision, A11.4 (Pittsburgh, PA, 2008).
12. R. I. Dennington, T. Keith, J. Millam, GaussV iew, Version 5.0.8, Semichem. Inc. Shawnee Mission, KS (2008).
13. A. D. Becke, Phys. Rev. A **38**, 3098 (1988). https://doi.org/10.1103/PhysRevA.38.3098
14. A. D. Becke, J. Chem. Phys. **98**, 5648 (1993). https://doi.org/10.1063/1.464913
15. C. Lee, W. Yang, and R. G. Parr, Phys. Rev. B **37**, 785 (1988). https://doi.org/10.1103/physrevb.37.785
16. T. Sundius, Vib. Spectrosc. **29**, 89 (2002). https://doi.org/10.1016/S0924-2031(01)00189-8 MOLVIB: A program for Harmonic Force Field Calculations, QCPE Program No. 807 (2002).
17. G. Varsanyi, Assignments for Vibrational spectra of seven Hundred Benzene Derivatives (Adam Hilger, London, 1974) **1-2**.
18. D. D. Parab and H. K. Kohli, J. Sci. Res. **17**, 547 (2025). https://dx.doi.org/10.3329/jsr.v17i2.75876
19. S. V. Chitra, A. Sankar, and K. Parimala, Indian Chem. Soc. **100**, ID 101000 (2023). https://doi.org/10.1016/j.jics.2023.101000
20. K. Parimala and S. Manimegalai, J. Pure Appl. Phys. **60**, 662 (2022). https://doi.org/10.56042/ijpap.v60i8.63474
21. L. E. Fernandez, A. Ben Altabef, and E. L. Vaaretti, J. Mol. Struct. **612**, 1 (2002). https://doi.org/10.1016/S0022-2860(01)00940-1
22. G. Socrates, Infrared and Raman Characteristic Group Frequencies, Tables and Charts, 3rd Edition (Wiley, Chichester, 2001).
23. K. Nagarajan, N. Surumbarkuzhali, and K. Parimala, J. Indian Chem. Soc. **100**, ID 100927 (2023). https://doi.org/10.1016/j.jics.2023.100927
24. M. E. Tuttolomondo, L. E. Fernandez, A. Navarro, E. L. Varetti, and A. B. Altabef, Spectrochim. Acta **60**A, 611 (2004). https://doi.org/10.1016/S1386-1425(03)00269-5
25. S. V. Chitra, A. Sankar, and K. Parimala, J. Indian Chem. Soc. **100B**, ID 101092 (2023). https://doi.org/10.1016/j.jics.2023.101092
26. K. Fukui, Theory of Orientation and Stereoselection, 1st Edition (Springer-Verlag, Berlin, 1975).
27. D. G. Iraiyadian, S. J. Vedhagiri, M. Govindarajan, and K. Parimala, Mater. Today: Proc. **60**, 1712 (2022). https://doi.org/10.1016/j.matpr.2021.12.236
28. H. M. Robert, D. Usha, M. Amalanathan, R. R. J. Geetha, and M. S. M. Mary, J. Mol. Struct. **1223**, ID 128948 (2021). https://doi.org/10.1016/j.molstruc.2020.128948
29. T. A. Koopmans, Physica **1**, 104 (1933). https://doi.org/10.1016/S0031-8914(34)90011-2